JOURNAL OF MAPS
2024, VOL. 20, NO. 1, 2394502
https://doi.org/10.1080/17445647.2024.2394502

Taylor & Francis
Taylor & Francis Group

Science

The geological setting of Matra ore deposit (France): insights from lithostratigraphy and polyphase deformation history

Danis Ionut Filimon [a], Giacomo Vannucci[a], Alessandro La Rosa [a], Vincenzo Zarone[b] and Maria Di Rosa [a]

[a]Dipartimento di Scienze della Terra, Università di Pisa, Pisa, Italy; [b]Dipartimento di Economia e Management, Università di Pisa, Pisa, Italy

ABSTRACT

Arsenic sulfide mineralization in Matra mine (southern Alpine Corsica) is hosted by two tectonic units belonging to the Schistes Lustrés Complex. Country rocks include a Jurassic ophiolitic sequence and related sedimentary covers, which were metamorphosed. Geological mapping and thin section analysis were used to understand lithostratigraphy and the tectononic-metamorphic history. The polyphase deformation history includes four phases of ductile deformation during the Late Cretaceous–Early Oligocene Alpine orogeny, with associated high-pressure–low-temperature metamorphism culminating in eclogite facies. The post-Alpine phase includes an N–S extensional fault system that controls the movement of ore fluids.

Key Policy Highlights:

- In the Matra area, the Santo Pietro di Tenda (ophiolitic sequence and sedimentary covers) and the Upper Castagniccia (sedimentary covers) Units crop out.
- They were involved in Alpine subduction registering a polyphase deformation and a peak metamorphism recorded in eclogite facies.
- The post-Alpine, N–S-trending normal fault of Matra hosts As-sulfide mineralization was exploited in the 1900s.

ARTICLE HISTORY
Received 31 January 2024
Revised 2 August 2024
Accepted 15 August 2024

KEYWORDS
Field mapping; ductile to brittle deformation; Matra fault; Schistes Lustrés Complex; Alpine Corsica

1. Introduction

The Matra mine was one of the most important sources of arsenic in France during the twentieth century (Orcel, 1921; 1924). Despite its significance, no detailed geological studies of the mine and surrounding area were ever completed. Therefore, the only available geological map is 1:50,000 scale (Caron et al., 1990), which lacks the necessary detail to understand the complex geology.

The Matra area underwent post-Alpine, N–S normal faulting that juxtaposed two tectonic units of oceanic affinity. These units are part of the Schistes Lustrés Complex (SLC), which was tectonically coupled and deformed during the Alpine orogeny (Elter & Pertusati, 1973; Malavieille et al., 1998; Molli, 2008; Schmid et al., 1996). The tectonic units composing the SLC experienced high pressure–low-temperature metamorphism (e.g. low-blueschist facies up to eclogite facies) caused by the Late Cretaceous–Early Eocene Alpine subduction event (Vitale Brovarone et al., 2013). Due to the intensity of deformation and metamorphism, a tectono-metamorphic reconstruction of the SLC is incomplete. Although select areas of the SLC were studied in the twenty-first century (Levi et al., 2007; Vitale Brovarone et al., 2013), these do not provide enough data to determine how the ore-controlling structures are related to periods of ductile (e.g. Alpine) or brittle (e.g. post-Alpine) deformation.

The current study was designed to address these deficiencies. Detailed field mapping of the Matra area provided data to create a 1:10,000 scale geological map. Changes to lithostratigraphy were made based on field observations and petrographic analyses of samples collected from different rock units. Whereas a polyphase deformation history was developed after structural analyses of field data and thin section study. Finally, cross-sections were generated showing important geological relationships to gain a better understanding of the N–S trending Matra Fault and mining site.

2. Geological setting

Rock formations in the Matra area are part of southern Alpine Corsica (Figure 1(a)) and underwent

CONTACT Danis Ionut Filimon danis.filimon@phd.unipi.it Dipartimento di Scienze della Terra, Università di Pisa, Pisa, Italy
Supplemental data for this article can be accessed online at https://doi.org/10.1080/17445647.2024.2394502.

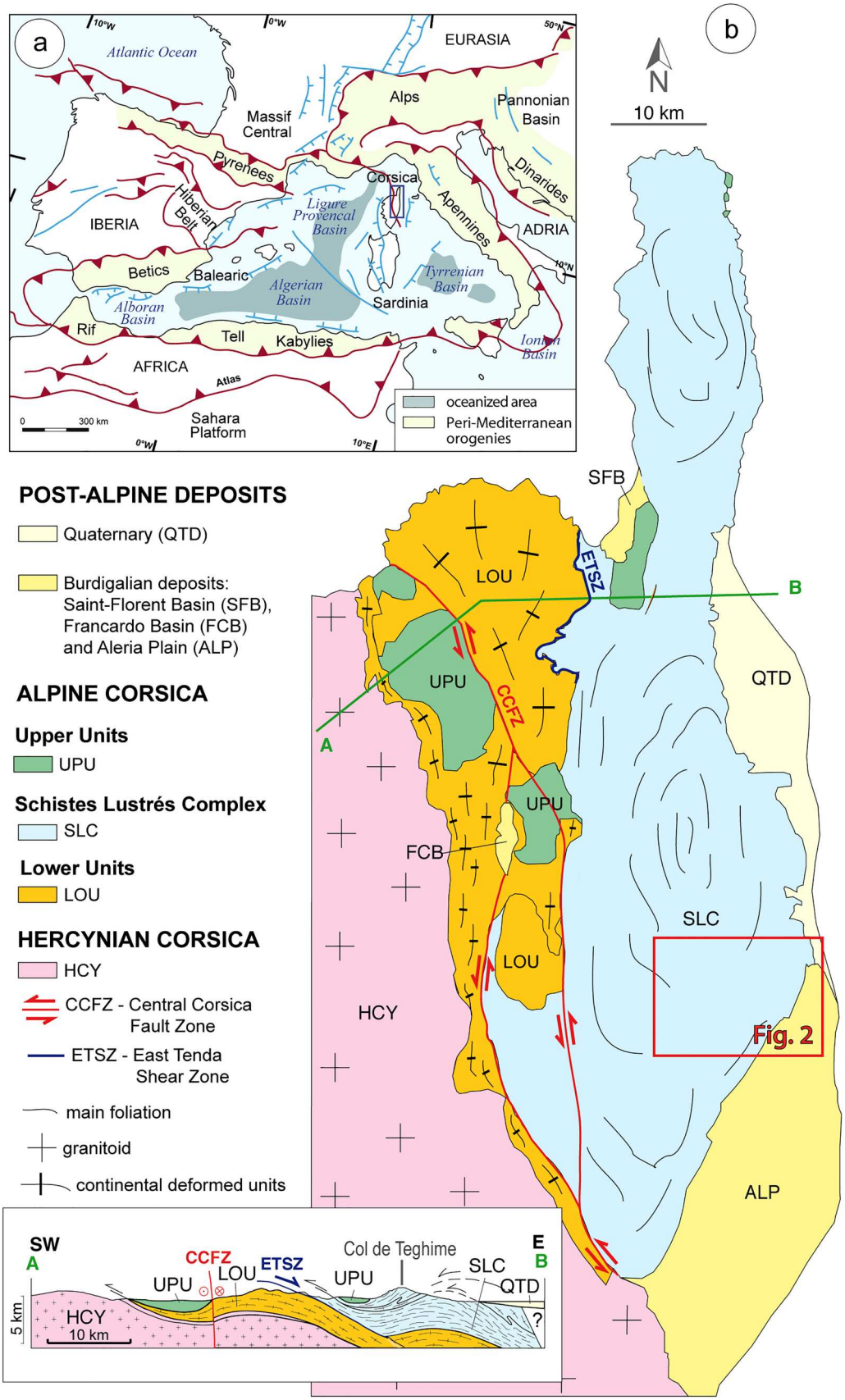

Figure 1. (a) Location of Corsica island in the western Mediterranean. (b) Tectonic map of northeastern Corsica (modified after Vitale Brovarone et al., 2013) and a schematic cross-section (not to scale, after Di Rosa et al., 2017). The location of the geological setting proposed and in the Main Map is indicated in the red box.

deformation and metamorphism during the Alpine orogeny (Durand-Delga, 1984). These formations consist of stacked continental and oceanic units, which have been divided into three groups of tectonic units (Figure 1(b)). The Lower Units represent part of the European continental margin that experienced

continental subduction, resulting in blueschist-facies metamorphism (Di Rosa, Frassi, Meneghini, et al., 2019). The middle SLC includes tectonic units of both oceanic and continental affinity that experienced low-grade blueschist to eclogite facies metamorphism (Vitale Brovarone et al., 2013) during Alpine subduction (Jolivet, 1993; Mattauer et al., 1981). The Upper Units consist of oceanic and continental rocks at the uppermost structural level of the unit pile that underwent very low-grade metamorphism (Durand-Delga, 1978). An important structural relationship to the W and SW records overthrusting of Hercynian Corsica, which represents the European continental margin, by Alpine Corsica (e.g. Durand-Delga, 1984). Note that only a narrow portion of Hercynian Corsica along its eastern boundary was involved in the Alpine orogeny (e.g. para-autochthonous units; Di Rosa, Frassi, Marroni, et al., 2020 and reference therein).

The current tectonic setting of Alpine Corsica is linked to rifting that started in the Middle Triassic–Early Jurassic. As rifting advanced to spreading between the European plate and the Adria microplate in Late Jurassic (Handy et al., 2010; Lagabrielle & Lemoine, 1997; Malusà et al., 2015), the Piemonte–Liguria Ocean formed. Then in the Late Campanian, closure of the Piemonte–Liguria Ocean occurred due to E-dipping intra-oceanic subduction (Marroni et al., 2017). As subduction continued from Middle–Late Eocene, it involved the ocean–continent transition zone and then the eastern rim of the European margin (Di Rosa, Frassi, Meneghini, et al., 2019; 2023; Maggi et al., 2012; Malavieille et al., 1998). However, an abrupt geodynamic change from compression to extension in the western Mediterranean occurred during the Early Oligocene (Chamot-Rooke et al., 1999). This caused a collapse of the newly created Alpine Corsica orogenic wedge and formation of the Ligurian–Provençal Basin (Gueguen et al., 1998). The extension was accompanied by the anti-clockwise rotation of the Corsica–Sardinia block toward the ESE (Malusà et al., 2015; Schmid & Kissling, 2000), which triggered the Apennine orogeny (Doglioni, 1991; Rosenbaum et al., 2002).

An important consequence of this rotation was the development of a sinistral strike-slip fault system known as the Central Corsica Fault Zone (CCFZ, Figure 1(b)). It occurs along the tectonic contact between Hercynian and Alpine Corsica (Lacombe & Jolivet, 2005; Maluski et al., 1973; Waters, 1990). The CCFZ post-dates ductile deformation associated with Alpine Corsica but pre-dates deposition of continental–marine deposits (e.g. the Aleria Plain, Saint-Florent and Francardo Basins) in the Burdigalian (Cavazza et al., 2007; Ferrandini et al., 1998; Gueydan et al., 2017). Extension during the Early Miocene was accommodated by normal faulting that moved

Figure 2. Geographic framework and tectonic sketch of the southern side of the Castagniccia dome (Alpine Corsica). Modified after Caron et al. (1990) by integrating field and DSM observations from the current study. The study area is indicated by the blue box. White dashed boxes indicate additional outcrops surrounding the mapped area in which the deformation history described for UCA and SPT units was also observed.

eastward in association with the rollback of the Apennine slab (Gueydan et al., 2017). Within the study area, extension produced an N–S fault system that includes the Presa Valley high-angle E-dipping normal fault (Figure 2), which hosts As sulfide mineralization. Mining activities peaked at 4000 t of As in 1913 with production from ~2 km of tunnels over four levels (Feraud, 1974), three entrances (i.e. Mining areas 1–3) and several shafts that are currently buried.

3. Methods

The study area is located in Presa Valley (42° 17'18.3"N, 9°23'22.5"E), north of Matra village. A structural analysis and detailed geological mapping were completed for an ~6 km^2 area around Matra, (hereafter referred to as Main Map, Figure 2). The field mapping was conducted at a 1:10,000 scale, with geological and structural elements recorded on topographic maps (elevation contours) generated from a 1-m LiDAR Digital Surface Model (DSM). Salient information about the rock types and their occurrence were used to compile synthetic lithostratigraphic logs. The rocks comprise two tectonic units: the Santo Pietro di Tenda (SPT) and the Upper Castagniccia (UCA; Figure 2).

The results of fault mapping in the field were augmented with remote mapping using a 1-m hillshaded DSM. This was done to determine the lateral extension of observed structures and identify additional faults in an ~36 km^2 area, which was mostly inaccessible. Evidence of active faulting was not observed in the study area, which was expected due to low present-day strain rates in Corsica (Serpelloni et al., 2005). Therefore, the structural analysis is based on the results of micro- and macroscale studies. Data generated through the petrographic study of thin sections were used to constrain micro-deformation and associated metamorphism. Morphological elements including scarps and zones of brittle fracturing, with trends similar to nearby faults, provided additional information to develop a deformation history of the SPT and UCA. When combined with structural measurements of fold axes (A2–A4), axial plane foliations (S2–S4), and faults that are presented on stereographic projections (Main Map), a polyphase deformation history was established. Note that numbers represent chronological phases in the deformation history. Therefore, different aspects of Phase 2 would include A2, S2, D2, etc.

4. Results

4.1. Lithostratigraphy

Bedrock in the study area consists of the UCA and SPT, which are two tectonic units of the SLC. The

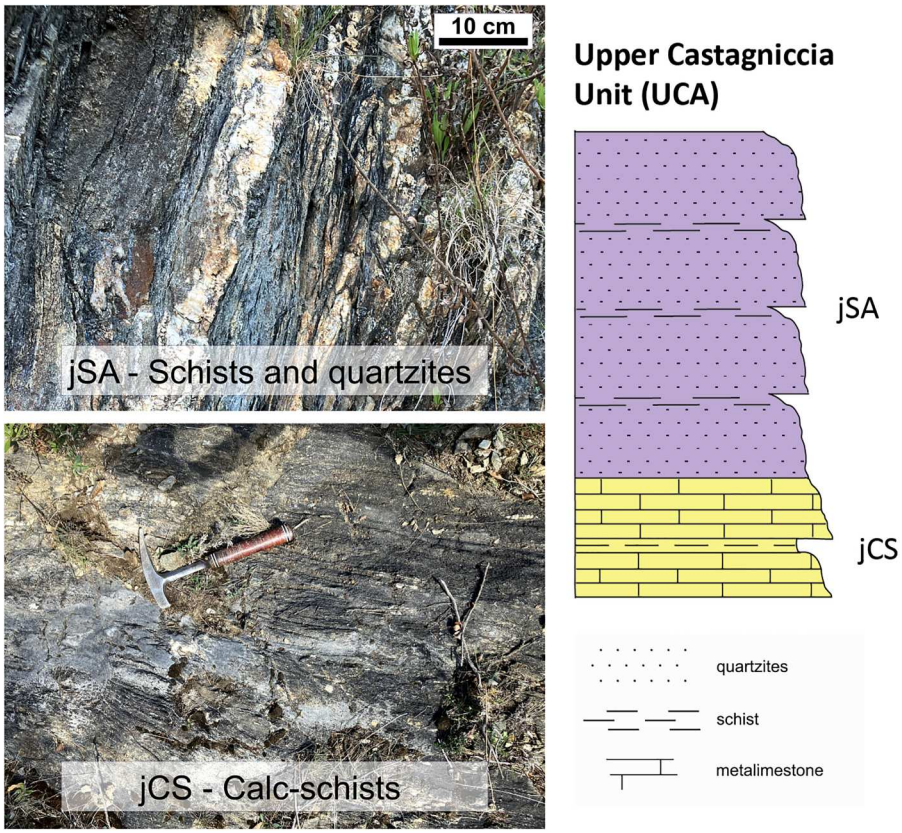

Figure 3. Stratigraphic log of the Upper Castagniccia Unit and mesophotographs of the different rock types cropping out in the study area.

UCA is composed of metamorphosed sedimentary rocks that include calc-schists (jCS, 30 m-thick) topped by schists and quartzites (jSA, up to 90 m; Figure 3). The calc-schists are impure metalimestones and contain phyllosilicate-bearing layers. In contrast, the schists and quartzites are characterized by alternating 2 cm to 10-cm-thick layers of quartzite and phyllosilicates. The age of these rocks is debated because high-pressure (HP) metamorphism destroyed biostratigraphic markers required for age dating. Caron et al. (1990) proposed a Jurassic age for the UCA, but a Cretaceous age is suggested by correlation with the same tectonic unit in the Corte sheet (Rossi et al., 1994).

The SPT is characterized by an ophiolitic sequence and related sedimentary cover (Figure 4). These Jurassic ophiolites are recognized as a sequence of 120-m-thick metaserpentinites (Λ) that contain <30 m thick sections of metagabbros (ΘS). Lenses of metaophicalcites (Oc) occur sporadically in Presa Valley close to the mining area 2 (Main Map). At their top is a thick sequence of metabasalts (≤100 m) that can be massive or pillowed (Σ). East of buildings in mining area 3 is a discontinuous layer of ophiolitic metabreccias (Ob) that have a maximum thickness of 50 m. Whereas the sedimentary cover rocks consist of metalimestones (jLM) and schists (jSC). The 30-m-section of metalimestones has a thick

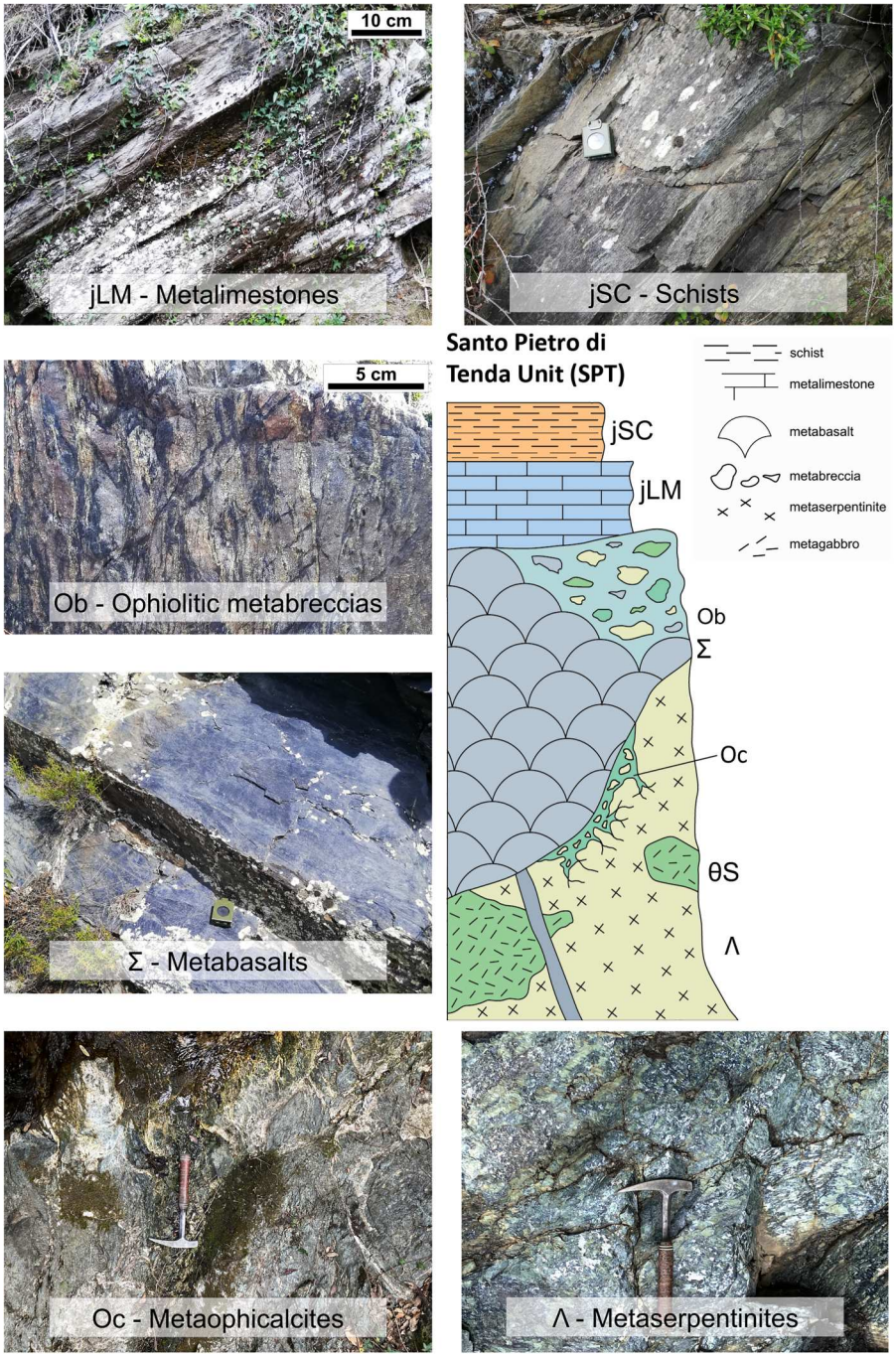

Figure 4. Stratigraphic log of the Santo Pietro di Tenda Unit and mesophotographs of the different rock types cropping out in the study area.

phyllosilicate-bearing base layer that becomes intermixed with and then replaced by metacarbonates at the top. Overlying this is a 20-m-thick section of garnet-rich mica-schists. A Late Jurassic–Early Cretaceous age for the sedimentary cover rocks was proposed by Caron et al. (1990).

4.2. Alpine deformation and metamorphism

Prominent geological features in the study area are NNW–SSE trending ductile structures. These formed as a result of polyphase syn-Alpine deformation (D1–D4) affecting the UCA and SPT units (Main Map). Due to this complex structure, additional data was obtained by studying samples at the meso - and microscopic scales to better understand the area's deformational history. The only evidence of D1 identified in hand samples of UCA is relict S1 foliation preserved by microlithons within hinges of F2 folds involving schists and quartzites. Whereas D2 is evident in all the rock types within both the UCA and SPT (Figure 5). Specifically for rocks of the UCA, an NW–SE trending S2 foliation can be classified as a mylonitic pervasive foliation that formed along the axial plane of F2 folds. By comparison, the deformation of rocks in the SPT produced non-cylindrical, isoclinal F2 folds characterized by acute hinges (Figure 6(a)), with syn-D2 shear zones parallel to the S2 foliation identified in metaserpentinites, e.g. along the D16 road at the beginning of the touristic trail (Main Map). In these shear zones, the strain is partitioned into 80 cm thick bands in which the core (~10 cm) and the damage zone show protomylonitic and foliated cataclasite fabrics, respectively.

Further study of D2 structures indicates they were deformed by closed, non-cylindrical F3 folds observed in both the SPT and UCA (Figure 6(b–d)). By plotting field data for A3 axes, a coherent NW–SE trend was identified (Figure 5). The related S3 axial plane foliation noted in schists and quartzites of UCA, as well as in schist of the SPT can be classified as spaced cleavage. The dispersion observed in the stereographic projections related to the D3 phase is due to the subsequent D4 folding phase, which is characterized by open to close folds with S4 sub-horizontal axial plane foliation classifiable as spaced fracture cleavage (Figure 6(e)). The interference pattern of type 3 in the Ramsay classification (1967) is evident in Figure 6 (f).

Microlithons in calc-schists of the UCA (Figure 7 (a)) preserve S1 foliation; recognized by phyllosilicates and calcite that underwent dynamic recrystallization. The S1 foliation was also identified in the matrix of ophiolitic metabreccias and microlithons preserved in the hinge zones of metabasalts within the SPT. Whereas the S2 foliation was identified in all the rock types of the UCA and SPT, as a pervasive and continuous foliation showing shear fabrics ranging from protomylonitic–ultramylonitic (Figure 7(b)), with associated dynamic recrystallization of phyllosilicates and amphiboles. Specifically, in calc-schist of the UCA an assemblage of white mica–quartz–albite–calcite occurs along the S2 foliation. The quartz displays

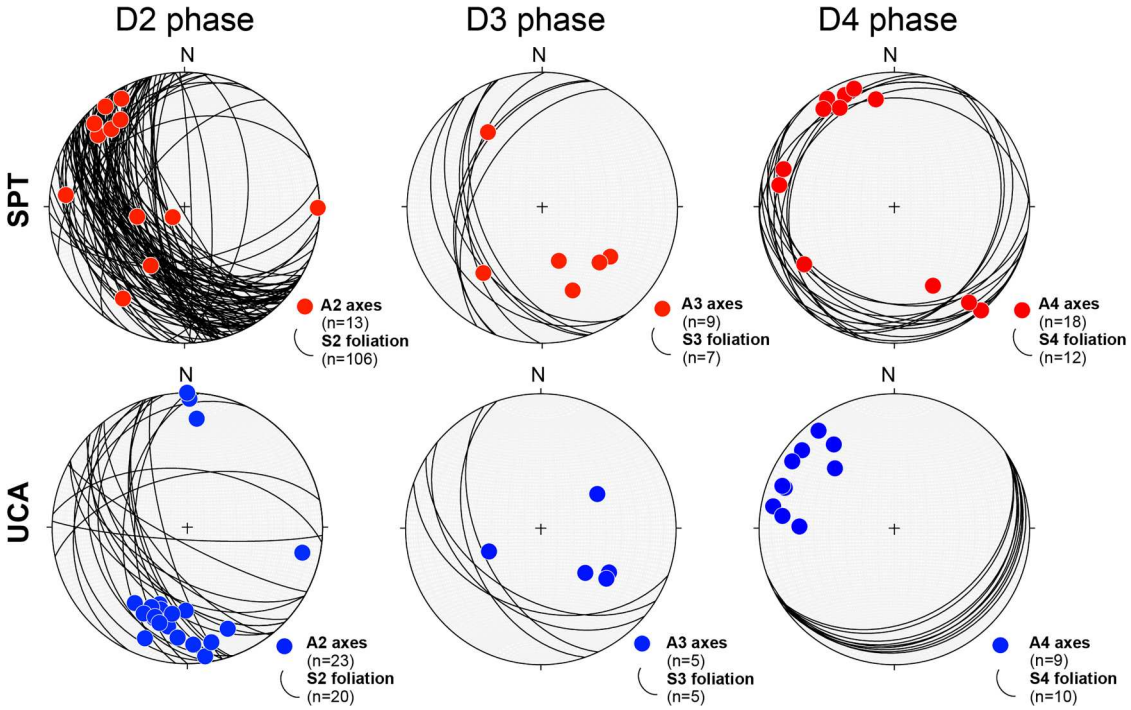

Figure 5. Stereographic plots of field data collected in the SPT and UCA for different phases of ductile deformation (Schmidt net projection, lower hemisphere). Key: S2, S3 and S4 foliation are related to the D2, D3 and D4 phases; axes of A2, A3 and A4 are related to the D2, D3 and D4 phases; n is the number of field measurements plotted.

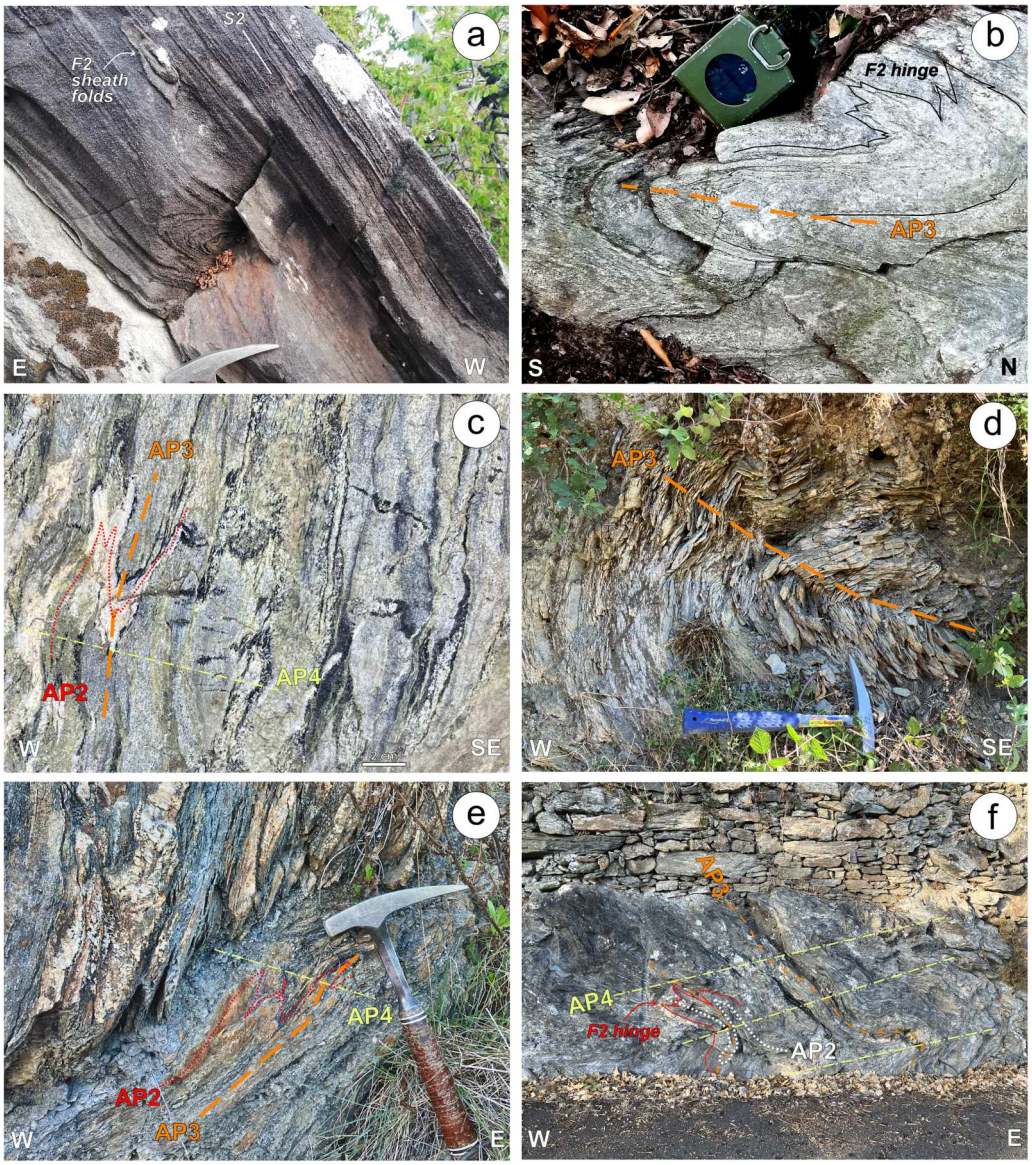

Figure 6. (a) F2 sheath fold in metalimestones of the SPT. (b) Relation between S2 and S3 axial plane foliations in metalimestones (SPT). (c) S4 axial plane foliation folding S2 and S3 foliations in the ophiolitic metabreccias (SPT). (d) Example of S3 axial foliation folding the S2 foliation of the calc-schists (UCA). (e) Example of S4 axial plane foliation folding the S2 and S3 foliation of the schists and quartzites (UCA). (f) D2–D3–D4 interference pattern in the calc-schist (UCA).

high-temperature fabrics such as Grain Boundary Migration (GBM, Figure 7(c)) and Subgrain Rotation (SGR) that indicate temperature ranges of 500–600°C and 400–500°C (Law, 2014), respectively. In contrast, the main anisotropy documented for the SPT is a composite S1 + S2 foliation recognized in metabasalts by the oriented growth of garnet, Na-amphibole, albite and epidote. Disequilibrium conditions are supported by Ca-amphibole, minor chlorite, and albite replacing the original blue amphibole and epidote. Therefore, the main anisotropy within the SPT is most likely related to metamorphism and deformation during late D2.

Shear domains associated with D2 were also recognized in metagabbro. These have a mylonitic foliation (e.g. S2 foliation), with a mineral assemblage of white mica–chlorite–albite that contains relicts of Na-pyroxene. Whereas garnet related to D2 in ophiolitic metabreccias has a coronitic texture that contains feldspar, Fe- and Ti-oxides and pyroxene (Figure 7(d)). This clearly indicates that garnet formed during peak metamorphism early in D2. Temperatures are interpreted to have been 400–600°C based on quartz microstructures (e.g. GBM, SGR) identified in the matrix of ophiolitic metabreccias (Law, 2014; Passchier & Trouw, 2005).

The microscopic study of samples affected by D3 and D4 indicates that no recrystallization occurred during either of these deformation events. However, late calcite and quartz veins do fill fractures that parallel AP3 and AP4 axial plane foliations.

4.3. Post-Alpine event

A post-Alpine extensional phase in the study area was identified using data from map-scale (Figure 8(a)) to

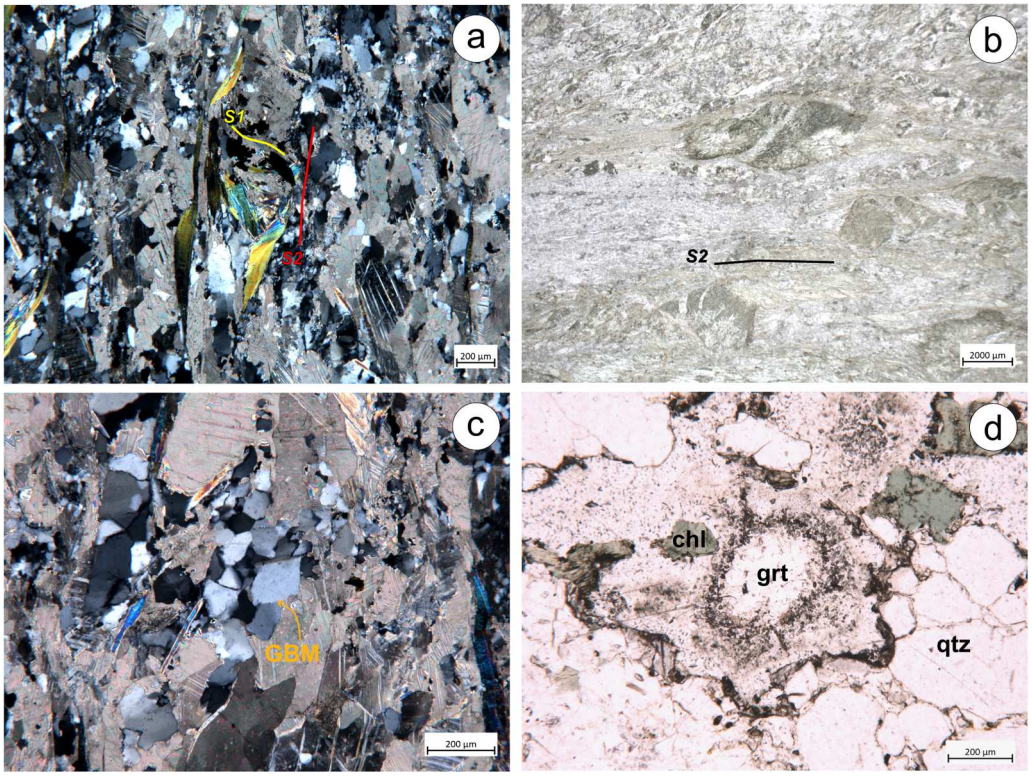

Figure 7. (a) Microphotographs (cross-polarized light) showing S1–S2 foliations marked by recrystallization of white mica in calc-schists, sample MAT 4 (UCA). (b) Relicts of Na-pyroxene within the S2 mylonitic foliation of a metagabbro, sample MAT 30 (SPT), plane-polarized light. (c) Grain boundary migration (GBM) textures of quartz in calc-schists, sample MAT 4 (UCA). (d) Relict garnet displaying a coronitic texture in ophiolitic metabreccia, sample MAT 1 (SPT), plane-polarized light.

mesoscale (Figure 8(b–d)) and microscale (Figure 8(e, f)). This brittle deformation is characterized by faults, joints, veins, and breccias. The NW–SE trending faults are part of a sinistral strike-slip system cut by normal faults that trend NNW–SSE and dip 70° E (Figure 8(a), Main Map). Normal fault kinematics are supported by down-dip slikenfibres composed of sulfides and quartz along the fault plane (Figure 8(e)). The normal faulting produced cataclasites ≤ 20-m-thick (Figure 8(c), Main Map). Cataclasite at a mesoscale is recognized as outcrops of gossan that are formed by the oxidation and leaching of sulfides through interaction with meteoric waters (Figure 8(d)). In contrast, shear structures at a microscale are characterized by ultra-cataclastic fabric, with microbreccia domains that consist of carbonate clasts surrounded by a carbonate matrix rich in sulfides. Silica injections veins cut the microbreccia domains. At the core of cataclasite zones, there is a pseudotachylite fabric consisting of dark, siliceous bands and injection veins that have distinct boundaries and contain angular microclasts of country rock (Figure 8(f)). The pseudotachylites are cut by late calcite veins (Figure 8(f)).

Veins in the ophiolitic rocks and calc-schists consist of calcite, quartz, and sulfides. The joints are set in a NE-SW oriented system, whereas the veins show a dispersion from N-S to NW-SE (Figure 8 (b)). An important point is that veins close to the main N–S normal fault in Presa Valley host ore are associated with matrix-supported breccias. The mineralization occurs in both the matrix and clasts. Sulfide minerals include realgar (As_4S_4), orpiment (As_2S_3), stibnite (Sb_2S_3), and pyrite (FeS_2) in a dolomitic and/or quartz gangue. Therefore, the main N–S normal fault in Presa Valley was most likely the ore-controlling structure.

The mapped extent of this fault was lengthened ~1 km to the north using DSM analysis, which identified additional linear structural elements. These trend ~N–S to ~NW–SE (Main map) and in some cases are represented by either scarps tens-to-hundreds of meters high or fracture systems that control the path of ephemeral river channels. A significant result to help establish age relationships between structures was the identification of a main N–S fault system that truncates an NW–SE trending fault (Bravone Fault in Figure 8(a)). The latter fault shapes a river valley and extends for ~14 km from west of Matra to the Aleria Plain (Figure 2, Main map).

5. Discussion and conclusions

Results of the current study justify making several changes to the established geology of the Matra area. Caron and Delcey (1979) proposed that calc-schist, schist, and quartzite were detached from a basement of oceanic affinity. This disagrees with the

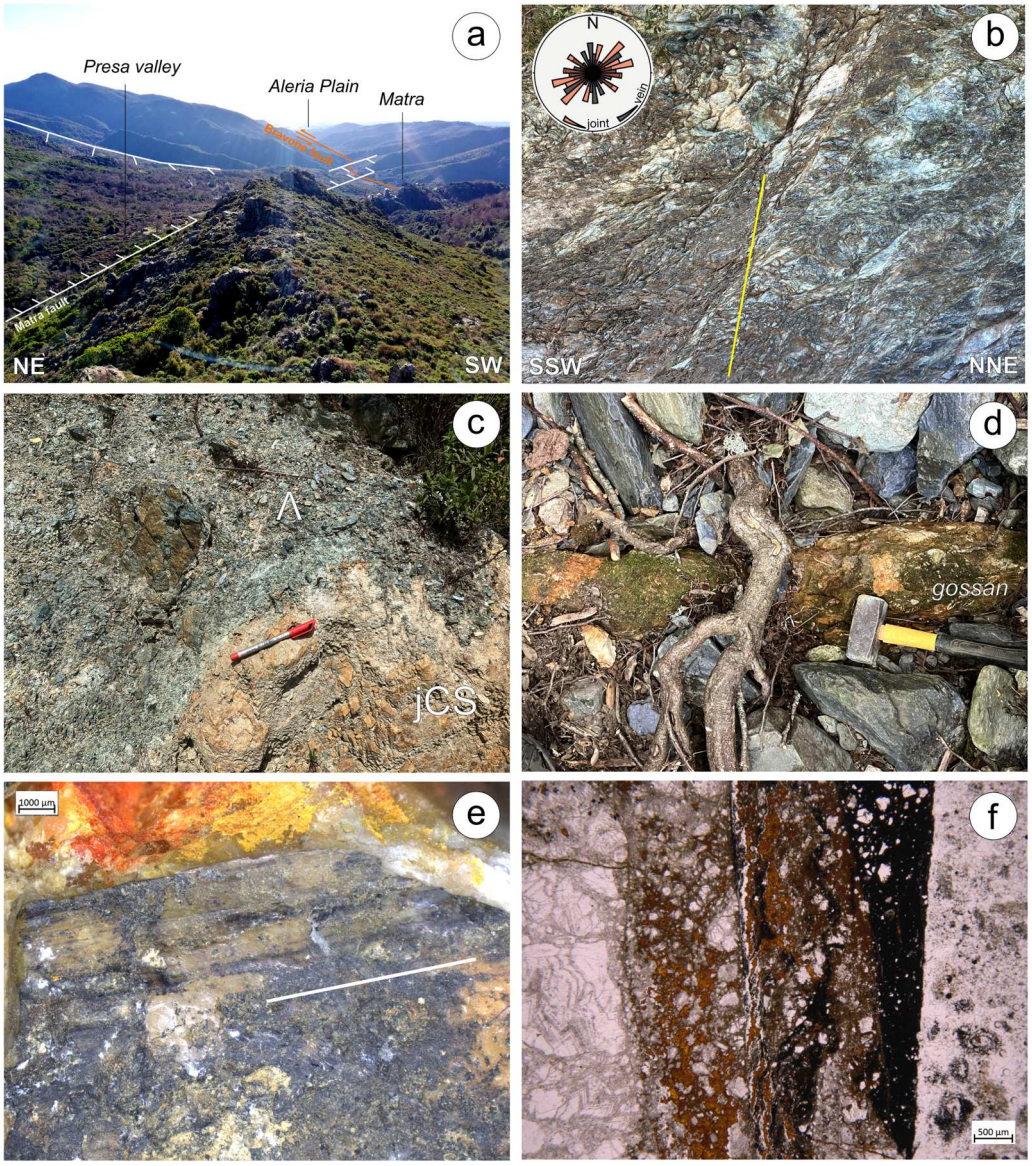

Figure 8. (a) Landscape view showing the main brittle structures in the study area. (b) Joint system in the metaserpentinites (SPT) and Rose diagram showing the distributions of field measurements for veins and joint/faults collected in the study area. (c) Damage zone occurring along the contact between metaserpentinite (Λ-SPT) and calc-schist (jSA-UCA). (d) Outcrop of gossan along Presa stream. (e) Slikenfibres on a mineralized fault plane, sample MAT 28. (f) Micro-shear zone showing the pseudotachylite fabric associated with a realgar and stibnite vein, sample MAT 9, plane-polarized light.

lithostratigraphy in a subsequent 1:50,000 geological map (Caron et al., 1990) showing extended outcrops, which are significantly reduced in the new 1:10,000 map. Results of the current study not only established a better coherence for the lithotypes of SPT but also identified metaophicalcites and ophiolitic metabreccias for the first time in Presa Valley. This new lithostratigraphy is similar to that presented by Levi et al. (2007) for the Lento Unit, which is an oceanic unit in the SLC. What could be the main lithostratigraphic difference between the two units involves their sedimentary cover rocks. These include metacherts and a thick sequence of calc-schist in the Lento Unit (e.g. the Erbajolo Fm.; Levi et al., 2007), compared with a 50-m-thick section of metalimestones and schists in the SPT.

The first attempt of tectono-metamorphic reconstruction of the Matra area is proposed in this work. Given the scarcity of the outcrops, in the main map, we propose an interpretation of the geology of the area, which takes into account the syn - and post-Alpine deformation. Four (D1–D4) ductile phases affected SPT and UCA. The D1 phase is rarely preserved due to being overprinted by D2, which represents the main deformation event. At the scale, syn-Alpine structures in D2 are recognized as synform and antiform megafolds (e.g. F2) in the SPT and UCA that have NNW–SSE striking axial planes. D2 was identified in all rock types and F2 folds are strongly non-cylindrical. Peak metamorphism occurred during phase D2, whereupon the exhumation of the UCA and SPT began.

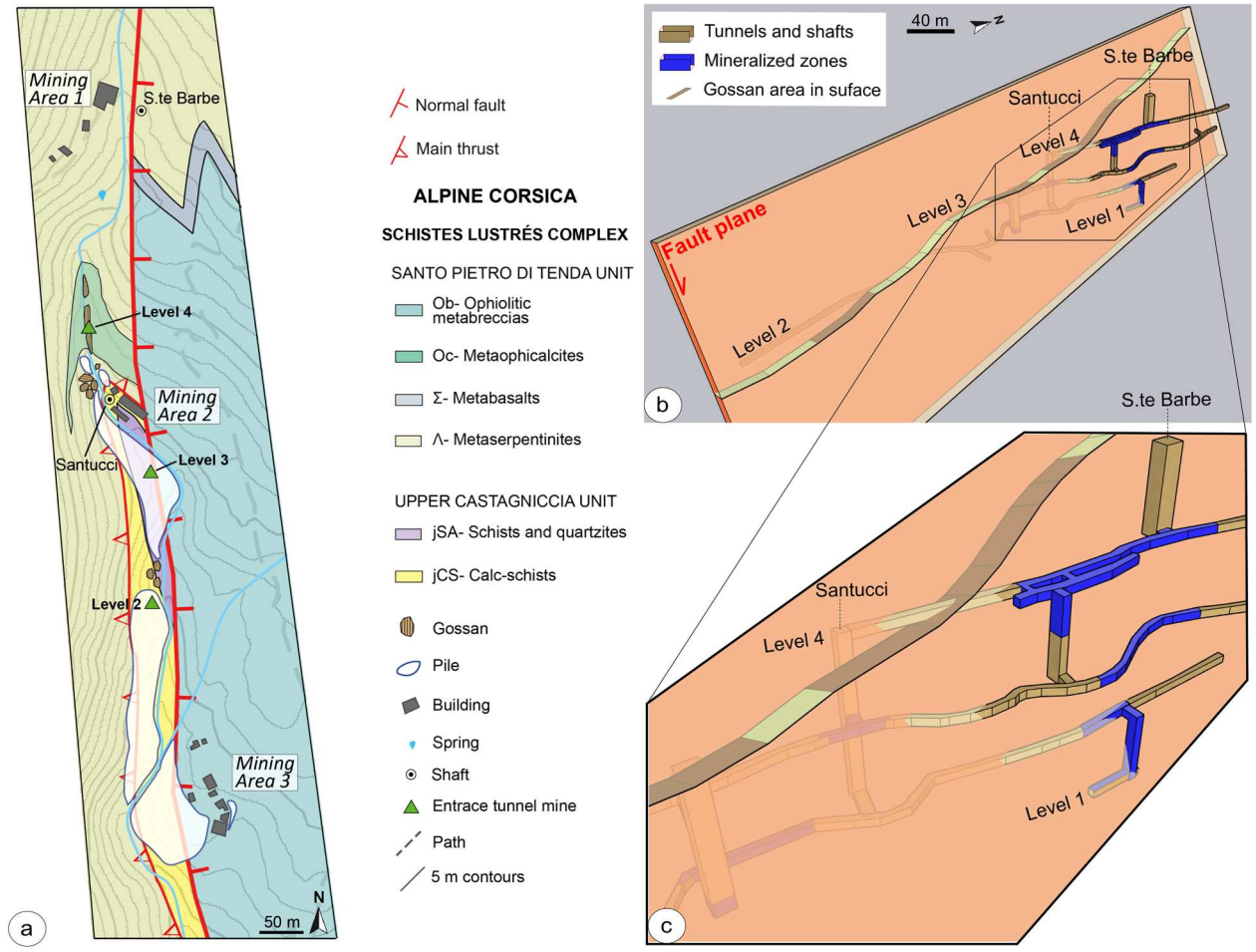

Figure 9. (a) Mining map of Matra. (b) 3D sketch model and (c) reconstruction of old mining reports (Feraud, 1974) that show how the different levels of tunnels all converge on the N–S trending normal fault.

These were subsequently deformed by the D3 and D4 events (Main Map). Folds produced by D3 have axial planes that strike NNW–SSE and dip ~70° W, which produces closed non-cylindrical synforms and antiforms. In contrast, A3 axes are slightly folded and dip to either the N or S (Figure 5). Deformation during D3 also includes top-to-E thrusts that crosscut the unit pile. The structures and textures that developed during D3 were in response to a compressional tectonic regime. Stress accommodation is recognized by E-verging folds and related AP3 axial plane foliation. The F3 folds might be associated with a back-thrusting stage within the orogenic wedge during horizontal shortening, as proposed by Levi et al. (2007) for the Lento Unit.

A change from compression to extension is recorded by D4 structures, such as open sub-horizontal folds that are related to the collapse of the Alpine orogenic wedge and correspond to the D3 phase observed in the Lower Units (Di Rosa et al., 2020). Work by Caron et al. (1990) at a larger scale in the region identified two Alpine metamorphic zones: a western characterized by lawsonite–glaucophane–garnet and eastern characterized by clinozoisite–glaucophane–garnet. Based on the results of the current study, these zones could reflect peak metamorphic conditions reached during D2 in the Presa Valley. Subsequent displacement along the prominent N–S trending normal fault locally juxtaposed the two zones in Presa Valley.

By combining the new lithostratigraphy and tectono-metamorphic history of the UCA and SPT, it is possible to better understand their place in the context of a regional tectonic setting for the SLC. Since units of the UCA occupied a basal position within the SLC tectonic pile, they experienced peak metamorphic conditions as recorded by the formation of eclogite (Caron & Peguinot, 1986; Delcey, 1974; Lahondère & Lahondère, 1988). By establishing this relationship, the SPT can be grouped into the Lower Slices Complex together with the Campitello, Morteda-Farinole, and Morteda Units. This is consistent with slices of meta ophiolites, metasediments, and metagranitoids that top the UCA (Dallan & Puccinelli, 1995; Lahondère & Guerrot, 1997).

All of these events predate As sulfide mineralization at the Matra mine, which occurred during post-Alpine brittle deformation. Results of both Caron et al. (1990) and the current study indicate a change in the extension and development of brittle structures. Mapping

at the 1:10,000 scale identified two main fault systems striking N–S and NW–SE. The former can be explained by a complex setting of extensional tectonics affecting Corsica Island during the opening of the Tyrrhenian Sea (Chamot-Rooke et al., 1999). This event was interpreted as the onset of Tyrrhenian rifting in the Langhian–Serravalian (Gueydan et al., 2017). An important point is that the N–S trending normal fault system postdates the NNW–SSE trending strike-slip CCFZ. This developed ~20 km west of Matra (Figure 1) and was active during the Oligocene (Maluski et al., 1973).

Regarding As sulfide mineralization, the N–S trending normal fault in Presa Valley was the main ore-controlling structure. This is based on several lines of evidence including a compilation of mining records that indicate production was localized on the normal fault (Figure 9). The main orebody had an N170° strike, easterly dip of 70° (Feraud, 1974 and reference therein), and was bounded by damages zones containing fragments of the SPT and UCA. Structural data and field relationships documented by the current study indicate As sulfide mineralization occurs in cataclastic zones proximal to a major N–S trending normal fault. Mineralization during activation of the fault is supported by sulfides in both breccia clasts and matrix, the restriction of gossan to the fault zone (Figure 8(d)), and slikenfibres of sulfides along the fault plane (Figure 8(e)). Therefore, fault movement allowed the circulation of fluids that deposited As sulfide ore.

Software

The elevation contour maps and hillshades used in this study were generated using the ArcGIS Pro® software. The whole Main Map has been georeferenced into a WGS 1984 World Mercator coordinate system (EPGS: 3395). The lithostratigraphic logs and the cross-sections were drawn with Adobe Illustrator and Inkscape, whereas the stereoplots were constructed with Stereonet Allmendinger v11.4.3. SketchUp software was used to reconstruct the mining tunnels.

Acknowledgements

The authors would like to thank the reviewers Makram Murad-al-shaikh, Rodolfo Carosi and Michel Ballèvre for their constructive suggestions and the editor Claudio Riccomini for the management. A special thanks to Rebecca Guelfi for her support during fieldwork. Michele Marroni and John Groff are always thanked for the constructive scientific exchanges and for the English editing service. This project benefited from the PRA 2022 project #20 (P.I. V. Zarone).

Disclosure statement

No potential conflict of interest was reported by the author(s).

Funding

This work was supported by PRA 2022 project #20 (P.I. V. Zarone).

Data availability statement

The 1 m RGE Alti® Digital Surface Models (DSMs) are provided by the Institute National de l'Information Gèographique e Forestière. The DSMs for the high Corsica are freely accessible and can be downloaded at the following link: https://geoservices.ign.fr/rgealti#telechargement1m. The structural data are available from the authors on request.

ORCID

Danis Ionut Filimon http://orcid.org/0009-0008-9610-4715
Alessandro La Rosa http://orcid.org/0000-0003-1858-1109
Maria Di Rosa http://orcid.org/0000-0002-1154-7429

References

Caron, J. M., & Delcey, R. (1979). Lithostratigraphie des Schistes Lustrés corses: diversité des séries post-ophiolitiques. *Comptes Rendus de Académié de Sciences Paris*, *288*, 1525–1528.

Caron, J. M., Loye-Pilot, M. D., Conchon, O., & Scius, H. (1990). Carte Géologique de la France, feuille Pietra-di-Verde (1115). BRGM, scale, 1:50000, 1 sheet.

Caron, J. M., & Peguinot, G. (1986). The transition between blue-schist and lawsonite bearing eclogites on the example of Corsican metabasalt. *Lithos*, *19*(3-4), 205–218. https://doi.org/10.1016/0024-4937(86)90023-X

Cavazza, W., DeCelles, P. G., Fellin, M. G., & Paganelli, L. (2007). The Miocene Saint-Florent Basin in northern Corsica stratigraphy, sedimentology and tectonic implications. *Basin Research*, *19*(4), 507–527. https://doi.org/10.1111/j.1365-2117.2007.00334.x

Chamot-Rooke, N., Gaulier, J. M., & Jestin, F. (1999). Constraints on Moho depth and crustal thickness in the Liguro-Provencal basin from a 3D gravity inversion: geodynamic implications. In B. Durand, L. Jolivet, F. Horvath, & M. Sérranne (Eds.), *The Mediterranean basin: Tertiary extension within the Alpine Orogen* (Vol. 156, pp. 37–61). Geological Society of London Special Publication.

Dallan, L., & Puccinelli, A. (1995). Geologia della regione tra Bastia e St-Florent (Corsica Settentrionale). *Bollettino della Società Geologica Italiana*, *114*, 23–66.

Delcey, M. R. (1974). Données sur deux nouvelles sèries litostratigraphiques de la zone des Schistes Lustrés de la Corse nord-orientale. *Comptes Rendus de Académié de Sciences Paris*, *279*, 1693–1696.

Di Rosa, M., De Giorgi, A., Marroni, M., & Vidal, O. (2017). Syn-convergence exhumation of continental crust: evidence from structural and metamorphic analysis of the Monte Cecu area, Alpine Corsica (Northern Corsica, France). *Geological Journal*, *52*(6), 919–937. https://doi.org/10.1002/gj.2857

Di Rosa, M., Frassi, F., Malasoma, A., Marroni, M., Meneghini, F., & Pandolfi, L. (2020). Syn-exhumation coupling of oceanic and continental units along the

western edge of the Alpine Corsica: A review. *Ofioliti*, *45* (2), 71–102.

Di Rosa, M., Frassi, C., Marroni, M., Meneghini, F., & Pandolfi, L. (2020). Did the "Autochthonous" European foreland of Corsica Island (France) experience Alpine subduction? *Terra Nova*, *32*(1), 34–43. https://doi.org/10.1111/ter.12433

Di Rosa, M., Frassi, C., Meneghini, F., Marroni, M., Pandolfi, L., & De Giorgi, A. (2019). Tectono-metamorphic evolution in the European continental margin involved in the Alpine subduction: new insights from the Alpine Corsica, France. *C.R. Acad. Sci. Paris*, *351* (5), 384–394.

Di Rosa, M., Sanità, E., Frassi, F., Lardeaux, J. M., Corsini, M., Marroni, M., & Pandolfi, L. (2023). A journey of the continental crust to and from the mantle depth: The P-T-t-d path of Venaco Unit, Alpine Corsica (France). *Geological Journal*, *59*(2), 422–440. https://doi.org/10.1002/gj.4872

Doglioni, C. (1991). A proposal for the kinematic modelling of W-dipping subductions - possible applications to the Tyrrhenian-Apennines system. *Terra Nova*, *3*(4), 423–434. https://doi.org/10.1111/j.1365-3121.1991.tb00172.x

Durand-Delga, M. (1978). *Corse. Guide de Géologie Regionaux*.

Durand-Delga, M. (1984). Principaux traits de la Corse alpine et corrélation avec les Alpes Ligures. *Memorie Della Società Geologica Italiana*, *28*, 285–329.

Elter, P., & Pertusati, P. C. (1973). Considerazioni sul limite Alpi-Appennino e sulle relazioni con l'arco della Alpi Occidentali. *Memorie della Società Geologica Italiana*, *12*, 359–375.

Feraud, J. (1974). *The arsenic sulfides ore deposits of south-eastern France: stratabound mineralisations and vein-type deposits* [PhD thesis, Laboratoire de Geologie appliquée, Université Pierre et Marie Curie, Paris VI].

Ferrandini, M., Ferrandini, J., Loye-Pilot, M. D., Butterlin, J., Cravatte, J., & Janin, M. C. (1998). Le Miocène du bassin de Saint-Florent (Corse): modalités de la transgression du Burdigalien supérieur et mise en évidence du Serravallien. *Geobios*, *31*(1), 125–137. https://doi.org/10.1016/S0016-6995(98)80102-2

Gueguen, E., Doglioni, C., & Fernandez, M. (1998). On the post-25 Ma geodynamic evolution of the western Mediterranean. *Tectonophysics*, *298*(1-3), 259–269. https://doi.org/10.1016/S0040-1951(98)00189-9

Gueydan, F., Brun, J. P., Phillippon, M., & Noury, M. (2017). Sequential extension as a record of Corsica Rotation during Apennines slab roll-back. *Tectonophysics*, *710-711*, 149–161. https://doi.org/10.1016/j.tecto.2016.12.028

Handy, M. R., Schmid, S. M., Bousquet, R., Kissling, E., & Bernoulli, D. (2010). Reconciling plate–tectonic reconstructions of Alpine Tethys with the geological–geophysical record of spreading and subduction in the Alps. *Earth-Science Reviews*, *102*(3-4), 121–158. https://doi.org/10.1016/j.earscirev.2010.06.002

Jolivet, J. (1993). Extension of thickened continental crust, from brittle to ductile deformation: examples from Alpine Corsica and Aegean Sea. *Annali di Geofisica*, *36* (2), 139–153.

Lacombe, O., & Jolivet, L. (2005). Structural and kinematic relationships between Corsica and the Pyrenees-Provence domain at the time of the Pyrenean orogeny. *Tectonics*, *24*(1), https://doi.org/10.1029/2004TC001673

Lagabrielle, Y., & Lemoine, M. (1997). Alpine, Corsican and Apennine ophiolites: the slow spreading ridge model. *CR Acad Sci Paris*, *325*, 909–920.

Lahondère, D., & Guerrot, C. (1997). Datation Sm-Nd du métamorphisme éclogitique en Corse alpine: un argument pour l'existence au Crétacé supérieur d'une zone de subduction active localisée sous le bloc corso-sarde. *Géologie de France*, *3*, 3–11.

Lahondère, J. C., & Lahondère, D. (1988). Organisation structural des "schistes lustrés" du Cap Corse (Haute-Corse). *Comptes Rendus de l'Académie des Sciences Paris*, *307*, 1081–1806.

Law, R. D. (2014). Deformation thermometry based on quartz c-axis fabrics and recrystallization microstructures: A review. *Journal of Structural Geology*, *66*, 129–161. https://doi.org/10.1016/j.jsg.2014.05.023

Levi, N., Malasoma, A., Marroni, M., Pandolfi, L., & Paperini, M. (2007). Tectono-metamorphic history of the ophiolitic Lento unit (northern Corsica): Evidences for the complexity of accretion-exhumation processes in a fossil subduction system. *Geodinamica Acta*, *20*(1-2), 99–118. https://doi.org/10.3166/ga.20.99-118

Maggi, M., Rossetti, F., Corfu, F., Theye, T., Andersen, T. B., & Faccenna, C. (2012). Clinopyroxene-rutile phyllonites from East Tenda Shear Zone (Alpine Corsica, France): pressure-temperature-time constraints to the Alpine reworking of Variscan Corsica. *Journal of the Geological Society*, *169*(6), 723–732. https://doi.org/10.1144/jgs2011-120

Malavieille, J., Chemenda, A., & Larroque, C. (1998). Evolutionary model for the Alpine Corsica: mechanism for ophiolite emplacement and exhumation of high-pressure rocks. *Terra Nova*, *10*(6), 317–322. https://doi.org/10.1046/j.1365-3121.1998.00208.x

Malusà, M. G., Faccenna, C., Baldwin, S. L., Fitzgerald, P. G., Rossetti, F., Balestrieri, M. L., Danisik, M., Ellero, A., Ottria, G., & Piromallo, C. (2015). Contrasting styles of (U)HP rock exhumation along the Cenozoic Adria-Europe plate boundary (Western Alps, Calabria, Corsica). *Geochemistry, Geophysics, Geosystems*, *16*(6), 1786–1824. https://doi.org/10.1002/2015GC005767

Maluski, H., Mattauer, M., & Matte, P. H. (1973). Sur la presence de decrochement alpins en Corse. *Comptes Rendus de Académié de Sciences Paris*, *276*, 709–712.

Marroni, M., Meneghini, F., & Pandolfi, L. (2017). A revised subduction inception model to explain the Late Cretaceous, double vergent oro- gen in the pre-collisional Western Tethys: evidence from the Northern Apennines. *Tectonics*, *36*(10), 2227–2249. https://doi.org/10.1002/2017TC004627

Mattauer, M., Faure, M., & Malavieille, J. (1981). Transverse lineation and largescale structures related to Alpine obduction in Corsica. *Journal of Structural Geology*, *3* (4), 401–409. https://doi.org/10.1016/0191-8141(81)90040-7

Molli, G. (2008). Northern Apennine-Corsica orogenic system: an updated overview. In S. Siegesmund, B. Fugenschuh, & N. Froitzheim (Eds.), *Tectonic aspects of the Alpine-Dinaride-Carpathian System* (pp. 413–442). Geological Society of London, Special Publication, 298.

Orcel, J. (1921). Le gisement de réalgar de Matra (Corse). *Bulletin de la Société française de Minéralogie*, *44*(4), 98–104. https://doi.org/10.3406/bulmi.1921.3761

Orcel, J. (1924). Notes minéralogiques et pétrographiques sur la Corse. *Bulletin de la Société des Sciences*

Historiques et Naturelles de la Corse, *XLIV*(461–464), 65–127. pl. I-XIII.

Passchier, C., & Trouw, R. A. (2005). *Microtectonics* (2nd ed.). Springer.

Ramsay, J. G. (1967). *Folding and fracturing of rocks*. McGraw-Hill.

Rosenbaum, G., Lister, G. S., & Duboz, C. (2002). Relative motion of Africa, Iberia and Europe during Alpine orogeny. *Tectonophysics*, *359*(1-2), 117–129. https://doi.org/10.1016/S0040-1951(02)00442-0

Rossi, P., Durand-Delga, M., Caron, J. M., Guieu, G., Conchon, O., Libourel, G., & Loÿe-Pilot, M. (1994). Carte Géologique de la France, feuille Corte (1110). BRGM, scale, 1:50000, 1 sheet.

Schmid, S., & Kissling, E. (2000). The arc of the western Alps in the light of geophysical data on deep crustal structure. *Tectonics*, *19*(1), 62–85. https://doi.org/10.1029/1999TC900057

Schmid, S. M., Pfiffner, O. A., Froitzheim, N., Schönborn, G., & Kissling, E. (1996). Geophysical–geological transect and tectonic evolution of the Swiss–Italian Alps. *Tectonics*, *15*(5), 1036–1064. https://doi.org/10.1029/96TC00433

Serpelloni, E., Anzidei, M., Baldi, P., Casula, G., & Galvani, A. (2005). Crustal velocity and strain-rate fields in Italy and surrounding regions: new results from the analysis of permanent and non-permanent GPS networks. *Geophysical Journal International*, *161*(3), 861–880. https://doi.org/10.1111/j.1365-246X.2005.02618.x

Vitale Brovarone, A., Beyssac, O., Malavieille, J., Molli, G., Beltrando, M., & Compagnoni, R. (2013). Stacking and metamorphism of continuous segments of subducted lithosphere in a high-pressure wedge: The example of Alpine Corsica (France). *Earth-Science Reviews*, *116*(1), 35–56. https://doi.org/10.1016/j.earscirev.2012.10.003

Waters, C. N. (1990). The Cenozoic tectonic evolution of Alpine Corsica. *Journal of the Geological Society*, *147*(5), 811–824. https://doi.org/10.1144/gsjgs.147.5.0811

The geological setting of Matra ore deposit (France): insights from lithostratigraphy and polyphase deformation history

Filimon D.I. [1*], Vannucci G. [1], La Rosa A. [1], Zarone V. [2], Di Rosa M. [1]

[1] Dipartimento di Scienze della Terra, Università di Pisa, Italy
[2] Dipartimento di Economia e Management, Università di Pisa, Italy

*Corresponding author: danis.filimon@phd.unipi.it

Dipartimento di Scienze della Terra
Università di Pisa

TECTONIC SKETCH

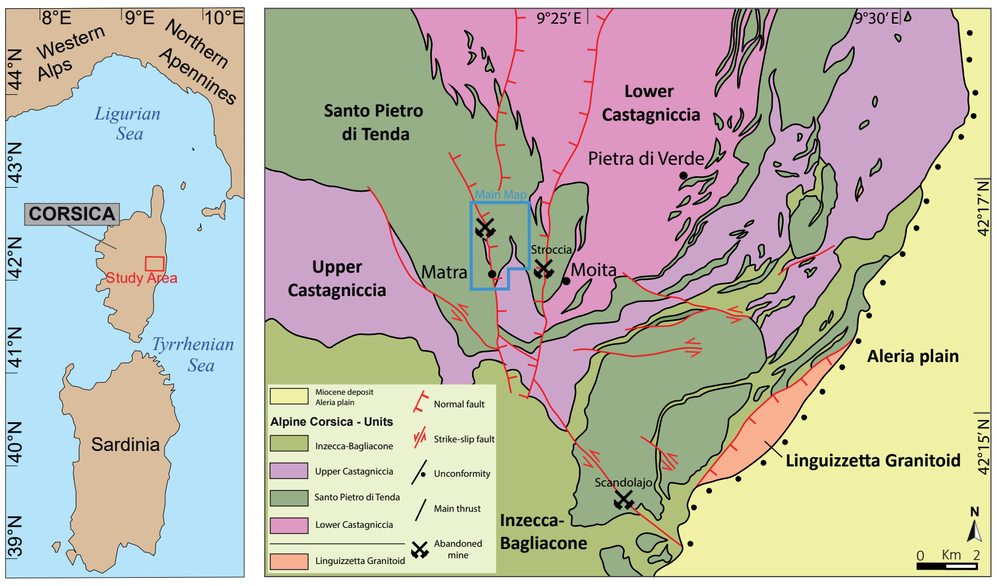

GEOLOGICAL MAP

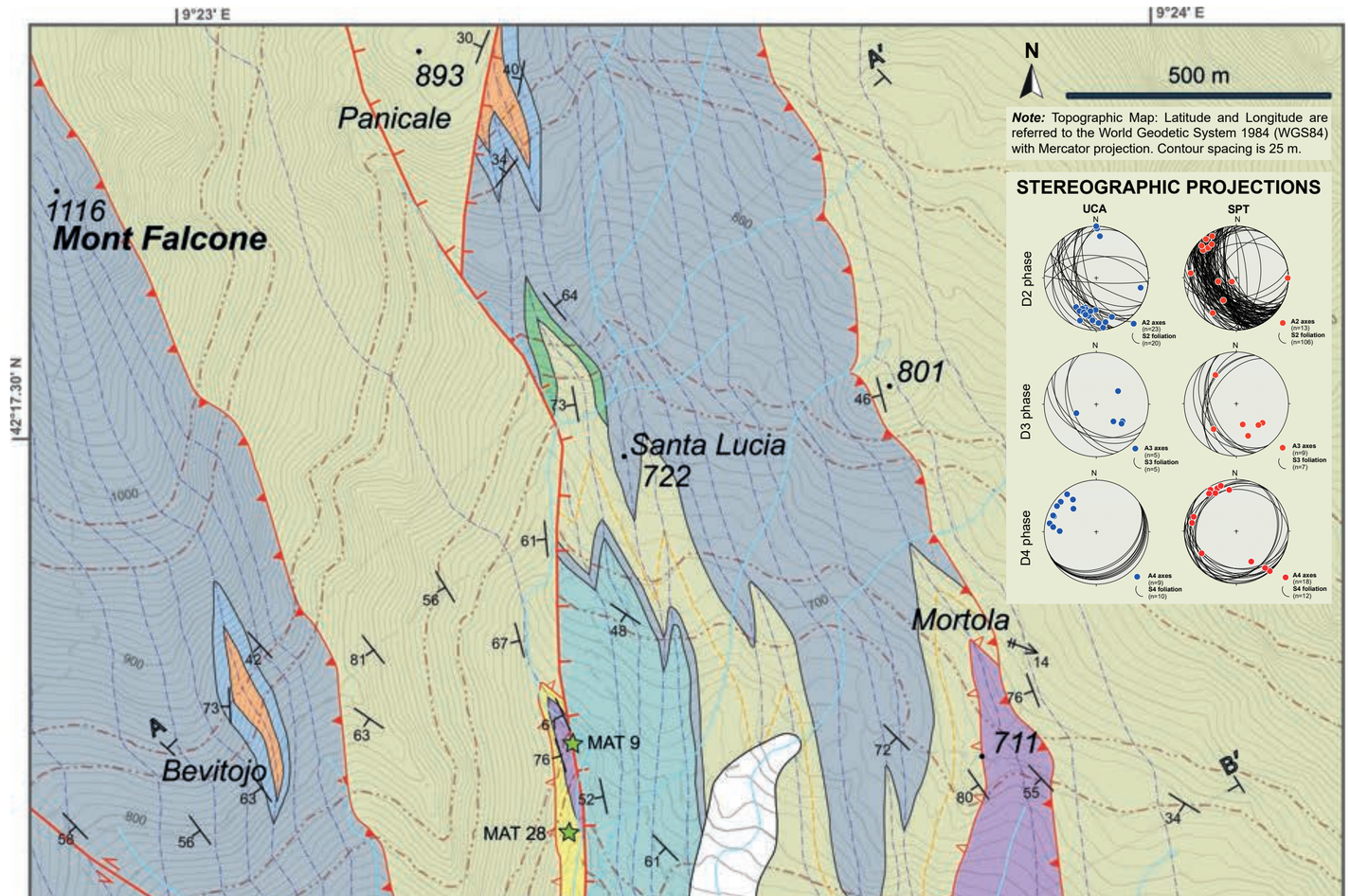

OUTCROPS

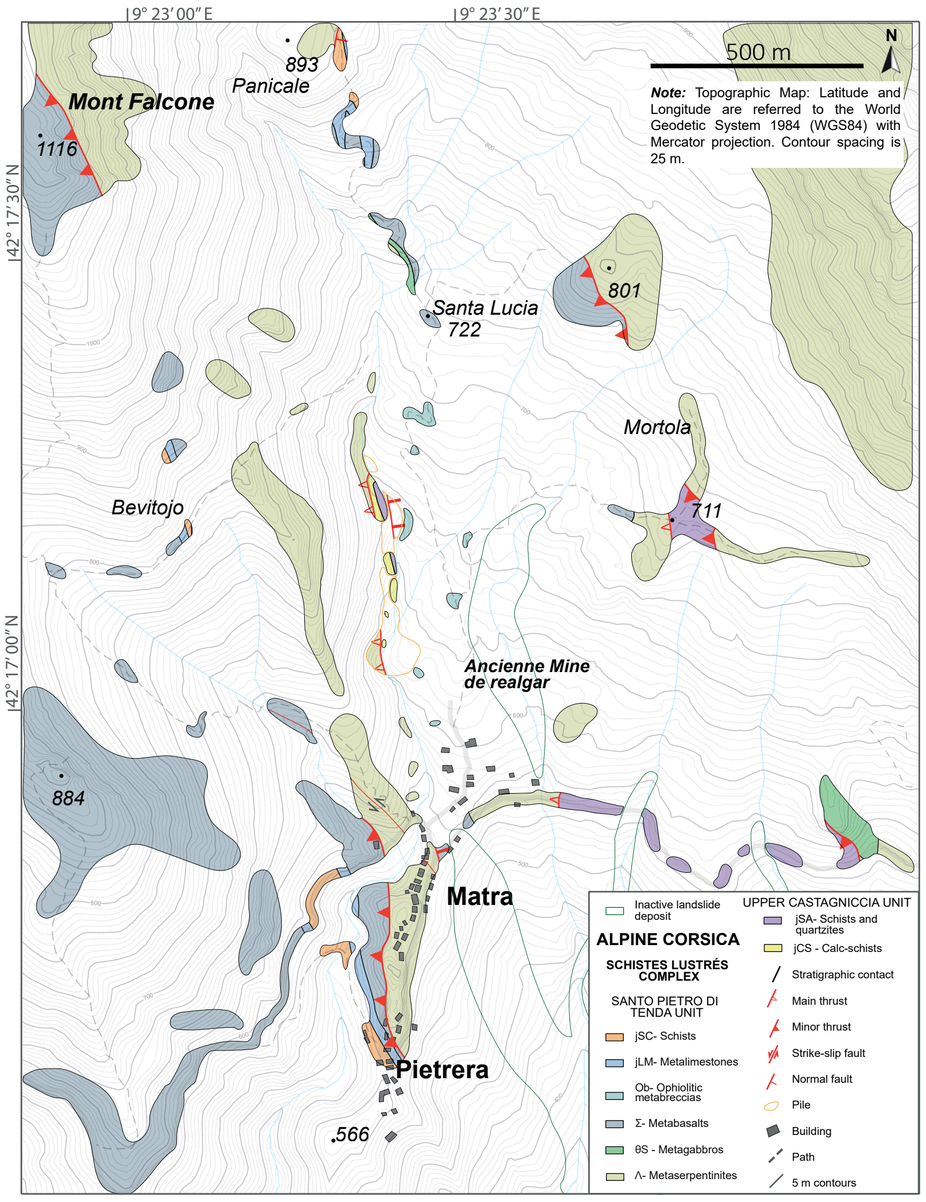

LITHOSTRATIGRAPHY

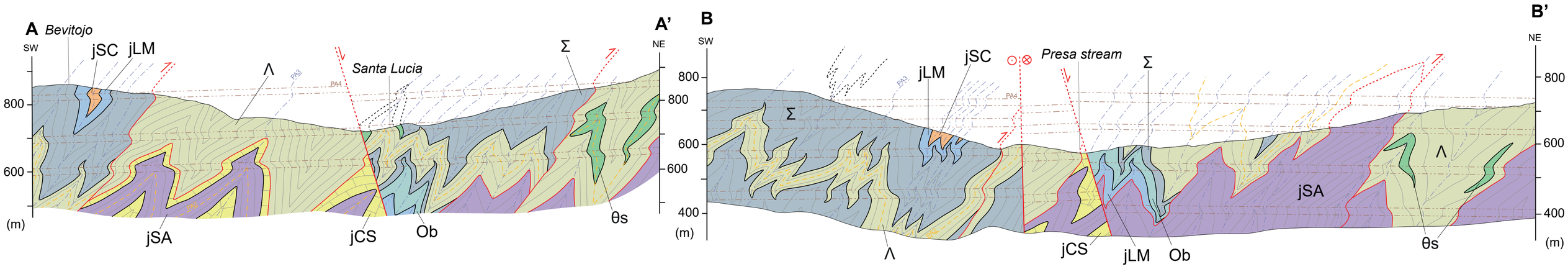

MINE AND GEOLOGY

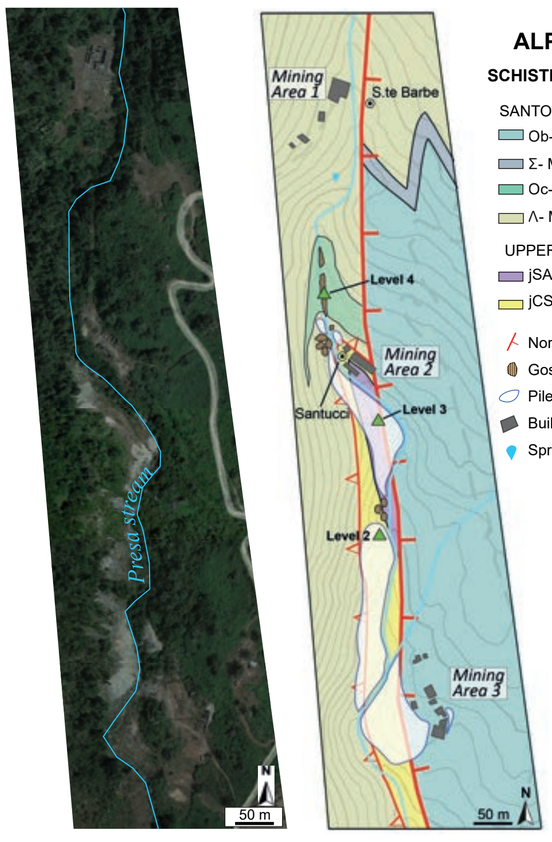

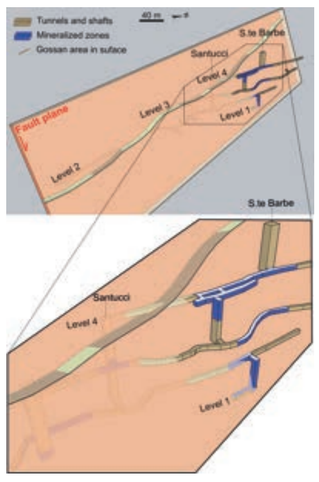

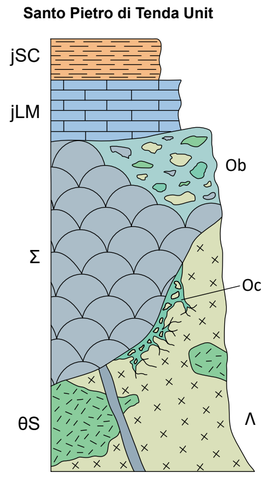

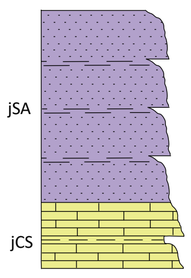

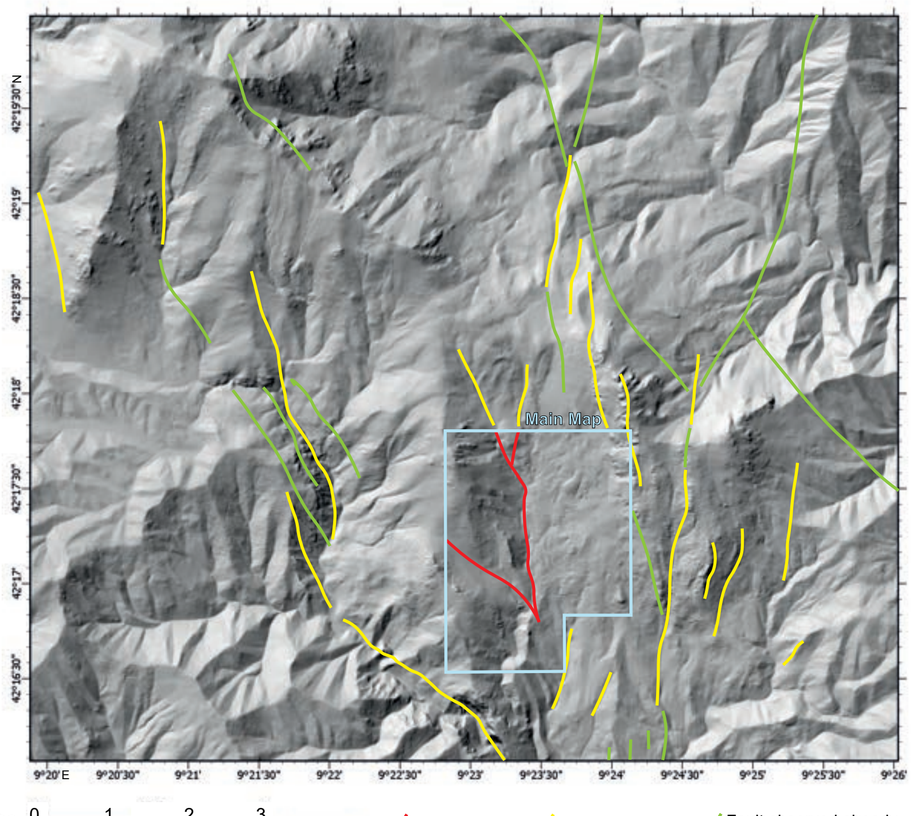

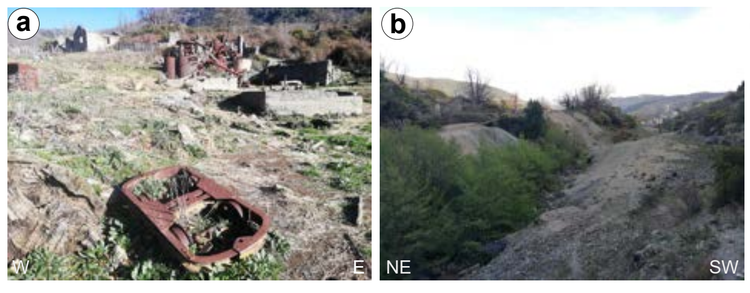

a) Mining Area 3, an area dedicated to ore washing, with several mining wrecks still visible. b) The different piles with the typical orange colour that characterizes the Presa stream. c) Rose diagram showing the distribution of veins and joint/faults in the study area.

INTERPRETATION OF BRITTLE STRUCTURES